Structure and magnetic properties of azido copper(II) complexes constructed from diamino ligands with different azido-bonding modes, nuclearity and dimensionality†

Salah S. Massoud,*[a] Febee R. Louka,[a] Tamim K. Haq,[a] Maher M. Henary,[b] Lindley Maxwell,[c] Alejandro Martín,[c] Eliseo Ruiz,[c] Ramon Vicente,*[c] Roland C. Fischer,[d] and Franz A. Mautner*[e]

[a] *Department of Chemistry, University of Louisiana at Lafayette, P.O. Box 43700 Lafayette, LA 70504, USA*

[b] *Department of Chemistry and Biochemistry, University of California, Los Angeles, CA 90095-1569, USA*

[c] *Departament de Química Inorgànica, Universitat de Barcelona, Martí i Franquès 1-11, 08028 Barcelona, Spain*

[d] *Institut für Anorganische Chemische, Technische Universität Graz, Stremayrgasse 9/V, A-8010 Graz, Austria*

[e] *Institut für Physikalische and Theoretische Chemie, Technische Universität Graz, A-8010 Graz, Austria*

(Received: , accepted:)

Keywords: Copper, Polynuclear Complexes, Azido bridged, Crystal structure, Magnetic properties

* Corresponding authors: E-mail: ssmassoud@louisiana.edu; Tel. +01 337-482-5672; fax: +01 337-482-5676 (SSM), E-mail: ramon.vicente@qi.ub.es (RM); Tel.: XXX; Fax: XXX and E-mail: mautner@ptc.tu-graz.ac.at; Tel. ++43 316-4873-8234; fax: ++43 316-4873-8225 (FAM).

Abstract

Four bridged-azido Cu(II) complexes were synthesized and structurally characterized: $[Cu_2(Et_3en)_2(\mu_{1,1}\text{-}N_3)_2(N_3)_2]$ (**1**), $[Cu_2(ip_2en)_2(\mu_{1,1}\text{-}N_3)_2(N_3)_2]$ (**2**), *catena*-$[Cu_2(Et_2Meen)_2(\mu_{1,3}\text{-}N_3)_3]ClO_4$ (**3**) and *catena*-$[Cu(ambza)(\mu_{1,1,3}\text{-}N_3)_2]$ (**4**), where Et_3en = *N*,*N*,*N*`-triethyl-1,2-diaminoethane; $ip_2en$ = *N*,*N*`-diisopropyl-1,2-diaminoethane; Et_2Meen = *N*,*N*-diethyl-*N*`-methyl-1,2-diaminoethane; ambza = 2-aminobenzylamine. Single crystal X-ray crystallography showed that complexes **1** and **2** are dinuclear with doubly bridged $\mu_{1,1}\text{-}N_3$, whereas **3** and **4** complexes consitute polymeric species with alternative sequence of single and double $\mu_{1,3}\text{-}N_3$ bridges for **3** with 1D chain, and triple $\mu_{1,1,3}$-briding azide in **4** with 2D extended structure. Variable temperature magnetic susceptibility over the temperature range 2-298 K revealed weak antiferromagnetic coupling (J = -1.8 cm^{-1}) for **1**, and ferromagnetic coupling with J values of 7.0 and 7.7 cm^{-1}, respectively for complexes **2** and **4**, respectively. Compound **3** shows a new topology for Cu(II) alternating chains $[Cu(1)(\mu_{1,3}\text{–}N_3)_2Cu(1')]\text{-}(\mu_{1,3}\text{–}N_3)\text{-}[Cu(2')(\mu_{1,3}\text{–}N_3)_2Cu(2'')]\text{-}(\mu_{1,3}\text{–}N_3)\text{-}[Cu(1)(\mu_{1,3}\text{–}N_3)_2Cu(1')]\text{-}\ldots$ The three different coupling constants have been obtained through fitting procedure and by DFT calculations. The magneto-structural properties of the complexes under investigation are discussed in relation to other related bridged-azido copper(II) complexes which are derived from closely diamino ligands.

Introduction

Azides are very toxic compounds to viruses and living cells including cells of bacteria, fungi as well mammalian cells and probably this may explain why these compounds have been used as preservative for vaccine in hospitals, poisons for pest control and as ingredients for certain drugs, like the anti-HIV medication AZT and AIDS.[1-3] In addition, the inorganic azides are known to decompose to produce nitrogen gas which is considered to be the base for automobile air bags.[4] Moreover, the azide ions are known to inhibit Cu containing metalloproteins (hemocyanin, ascorbate oxidase, tyrosinase) in biological systems.[5] Aside from the explosive nature of the azide materials, they still show some interesting applications and the simple azide ion, N_3^- due to its versatile coordination bonding properties have been extensively used to assemble and bridge *3d* divalent metal ions such Mn^{2+}, Fe^{2+}, Co^{2+}, Ni^{2+}, Cu^{2+} and Zn^{2+}, as well Cd^{2+} in a variety of ways.[6-16] Some of these compounds showed unique and unexpected topological structures.[6,8,17-25] The small nature of the ion, its linear shape, delocalization of its π-electrons on the three nitrogen atoms and its effectiveness to propagate the magnetic interaction between the paramagnetic centers, resulted in the formation of many coordination compounds of interesting magnetic properties, specifically with copper complexes.[18-45]

The azido ligand bridges metal ions in many different coordination bonding modes, probably the most common of which are the end-to-end (EE or $\mu_{1,3}$-N_3) and the end-on (EO or $\mu_{1,1}$-N_3). In general in copper(II) complexes, the former EE bonding mode usually leads to antiferromagnetic interaction, whereas the EO mode leads to ferromagnetic interaction.[26-43] Azido complexes composed of mixed bridging $\mu_{1,3}$-N_3 and $\mu_{1,1}$-N_3 were also reported in some compounds.[6,17,46-48] In addition to these bridging modes, the azido ligand exhibits a wide range of less common coordination modes that include triple-bridges $\mu_{1,1,3}$-N_3 and/or $\mu_{1,1,1}$-N_3,[18-22,31,43,45,48] tetra-bridges $\mu_{1,1,1,1}$-N_3 and $\mu_{1,1,2,2}$-N_3,[49,50] as well as hexa-bridges $\mu_{1,1,1,3,3,3}$-N_3.[33] These modes which have been summarized several times,[6(a),8(a),10(b),51] had led to the formation of diverse structures with different dimensionality (1D, 2D and 3D) and nuclearity (tri, tetra-, hexa- and poly-nuclear species)[6,21-23,25,48-50] as well coordination polymers.[1(b),18-24,26,27(a),30,31,33,34(a),35,39,43,45] The coordination bonding mode of the bridging azido ligand depends largely on the nature of the coordinated co-ligand(s) and the steric environments imposed into their skeletons and to some extent on the nature of metal ion and its oxidation state.[6,8,17]

In bridged Cu(II)-azido complexes, it has been reported that symmetric doubly bridging $\mu_{1,3}$-

azido bonding modes are strongly favor antiferromagnetic coupling, whereas the corresponding $\mu_{1,1}$-azido modes are strongly producing ferromagnetic when the Cu-N_{azide}-Cu angle is less than 108º. In contrast, while asymmetric doubly bridging $\mu_{1,3}$-azido bonding results in weak antiferromagnetic coupling, the corresponding $\mu_{1,1}$-azido bridges may propagate moderately strong ferro- or anti-ferromagnetic interactions.[7(c),8(c),9(a),14,17,52]

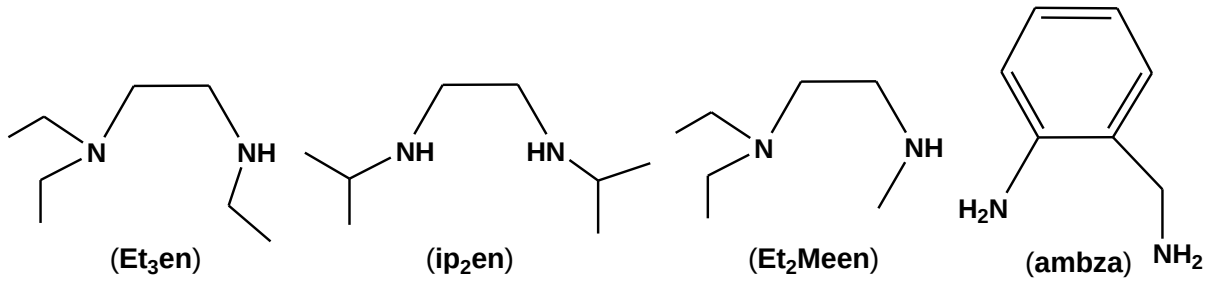

Chart 1. Structure of the diamino compounds used in this study

Herein we report the synthesis and structural characterization of some Cu(II)-azido complexes that derived from simple diamine ligands with different structural skeletons (*N*,*N*,*N*`-triethyl-1,2-diaminoethane, $Et_3$en; *N*,*N*`-diisopropyl-1,2-diaminoethane, ip_2en; *N*,*N*-diethyl-*N*`-methyl-1,2-diaminoethane, Et_2Meen; 2-aminobenzylamine, ambza) in an attempt to understand how the ligand environment might affect the coordination bonding mode of the bridged-azide and the magnetic properties of the resulting complexes. The structure formulas of the ligands used in this study are shown in chart 1. Results will be discussed in relation to other related similar systems (en, ??????????????????).

---

† Ligand abbreviations: Et_3en = *N*,*N*,*N*`-triethyl-1,2-diaminoethane; $ip_2$en = *N*,*N*`-diisopropyl-1,2-diaminoethane; Et_2Meen = *N*,*N*-diethyl-*N*`-methyl-1,2-diaminoethane; ambza = 2-aminobenzylamine; Me4en = *N*,*N*,*N*`,*N*`-tetraethyl-1,2-diaminoethane; en = 1,2-diaminoethane, Meen = *N*-methyl-1,2-diaminoethane, Eten = *N*-ethyl-1,2-diaminoethane, pren = N-n-Bu-1,2-diaminoethane, $Bz_2$en = N,N`-dibenzylamine, N,N-Et_2en = *N*,*N*-diethyl-1,2-diaminoethane, EtEt`-en = *N*,*N*`-diethyl-1,2-diaminoethane, Me_4en = *N*,*N*,*N*`,*N*`-tetramethyl-1,2-diaminoethane.

Results and discussion

Synthesis of the complexes

The synthesis of the four green bridged-azido Cu(II) complexes: $[Cu_2(Et_3en)_2(\mu_{1,1}\text{-}N_3)_2(N_3)_2]$ (**1**), $[Cu_2(ip_2en)_2(\mu_{1,1}\text{-}N_3)_2(N_3)_2]$ (**2**), *catena*-$[Cu_2(Et_2Meen)_2(\mu_{1,3}\text{-}N_3)_3]ClO_4$ (**3**) and *catena*-$[Cu(ambza)(\mu_{1,1,3}\text{-}N_3)_2]$ (**4**) was straight forward. The complexes were obtained in moderate yields (65-75%) by reacting a warm methanolic solution containing equivalent amounts of $Cu(ClO_4)_2\cdot 6H_2O$ or $Cu(NO_3)_2\cdot 3H_2O$ and the corresponding diamine with an aqueous solution of two equivalents of NaN_3, which was slowly added drop wise to minimize the possible formation of the brown insoluble $Cu(N_3)_2$ compound. Slow evaporation of the reaction mixtures at room temperature afforded the desired complexes. However, in case of complexes **3** and **4** the use of $Cu(ClO_4)_2$ led to the isolation of two unidentified azido products, therefore to ensure the formation of pure complexes $Cu(NO_3)_2$ was used instead of the perchlorate salt. The synthesized complexes were structurally characterized by elemental microanalyses, IR and UV-Vis spectra, conductivity measurements and single crystal X-ray crystallography. The magnetic susceptibilities of the complexes were also investigated at variable temperature (2-300 K). The molar conductivity, Λ_M of the complexes **1** and **2**, measured in CH_3CN revealed their non-electrolytic nature (Λ_M = 3-5 $\Omega^{-1}cm^2mol^{-1}$), whereas a value of 174 $\Omega^{-1}cm^2mol^{-1}$ was determined in **3** which is consistent with 1:1 electrolytic behavior.[53] The very low solubility of **4** in CH_3CN prohibits determining its Λ_M.

IR and electronic spectra of the complexes

The IR spectra of the four azido complexes **1**-**4** displayed some general features. They revealed weak absorption bands over the frequency ranges 3250-3160 and 2970-2890 cm^{-1} due to ν(N-H) of the amino group and the aliphatic ν(C-H) stretching vibrations, respectively. The weak band observed at 3115 cm^{-1} in complex **4** was assigned to the aromatic ν(C-H) stretching of ambza ligand. Also, the complexes displayed two or three strong absorption bands at the frequency region 2100-2020 cm^{-1} attributed to the asymmetric stretching vibration, $\nu_{as}(N_3)$ of the azido groups (see experimental section). In addition, the perchlorate complex **3** displayed two strong bands at 1120 and 1081 cm^{-1} due ν(Cl-O) of the perchlorate counter ion. The split of this band results from the reduction of the symmetry of the ClO_4^- ion to C_{3v} or C_{2v} due to its involvement in hydrogen bonding with the H-N of the amine ligand (see next section).

The visible spectra of the azido complexes **1**-**4** were recorded in CH_3CN. Complexes **1**-**3** displayed a single broad band over the wavelength range 600-630. In general, this feature is characteristic for *five-coordinate* Cu(II) complexes which often may or may not be associated with a

low-, or high-energy shoulder. In many cases, the broad band in the 550-660 nm range (dxz, dyz ⟶ dx^2-y^2) with a low-energy shoulder at λ > 800 nm indicates a square pyramidal (SP) geometry,[54] whereas the presence of a single d-d band at λ > 800 nm (dxy, dx^2-y^2 ⟶ dz^2) with a high-energy shoulder (spin forbidden, dxz, dyz ⟶ dz^2) is typical for trigonal bipyramidal (TBP) stereochemistry. Thus, based on this criterion, the electronic spectral data of the **1**-**3** complexes are more consistent with distorted SP, where the absorption maximum band observed in the visible region results from $^2B_1 \leftarrow {}^2E$ transition.[54] The visible spectrum of **4** revealed the presence of a broad absorption band at 638 nm with a shoulder ~570 nm. This spectrum is common for d^9 Cu^{2+} in strongly tetragonally distorted octahedral environment due to strong *Jahn-Teller* distortion. In the tetragonal field (close to D_{4h} symmetry) the transitions: $^2A_{1g} \leftarrow {}^2B_{1g}$, $^2B_{2g} \leftarrow {}^2B_{1g}$ and $^2E_g \leftarrow {}^2B_{1g}$ are expected but because the ligand field is weak, the splitting is small and hence the band is broadening.[55] The assigned geometries of the **1**-**4** complexes in solution are in complete agreement with those found in the solid states (see next section).

Description of the structures

$[Cu_2(Et_3en)_2(\mu_{1,1}\text{-}N_3)_2(N_3)_2]$ (**1**). A perspective view together with the partial atom numbering scheme for the neutral dinuclear title complex **1** is presented in Fig. 1(a), and selected bond parameters are summarized in Table 1. The copper(II) atoms within the centrosymmetric dinuclear unit are bridged by two azide ions in a $\mu_{1,1}$- end-on fashion. Each metal center is penta-coordinated by N(1) and N(2) donors of the Et_3en ligand, N(11) and N(11') of the two azide bridges and N(21) of a terminal azide group. The coordination polyhedron around copper(II) can be described as a distorted intermediate geometry, which is more close to square pyramid (SP) with an Addison parameter τ = 0.46.[56] The apical position is occupied by N(11') atom [Cu(1)-N(11') = 2.312(2) Å], and the basal Cu-N bond distances are in the range from 1.991(2) to 2.096(2) Å. The Cu(1)···Cu(1') distance is 3.3476(6) Å and the shortest inter-dinuclear metal-metal separation is 5.9612(9) Å. The Cu(1)-N(11)-Cu(1'), Cu(1)-N(11)-N(12), Cu(1')-N(11)-N(12) and Cu(1)-N(21)-N(22) angles are 101.77(9), 125.55(18), 125.60(17) and 128.48(19)°, respectively. The "out-of plane" angle N(11')···N(11)-N(12) is 156.7(3)°. The end-on bridging azide group is more asymmetric with a Δ(N-N) value of 0.057 Å compared to the terminal one with a Δ(N-N) value of 0.021 Å. The N-N-N bond angles of the azide ligands are 177.1(3) and 176.4(3)°. Hydrogen bonds of type N-H···N between N(2) donor atoms and adjacent N(23) acceptor atoms of terminal azide

groups connect the dinuclear subunits into a supramolecular 1D system oriented along the *b*-axis of the unit cell (Table 5, Fig. S1).

(a)

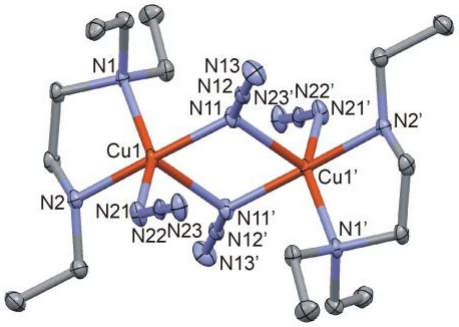

(**b**)

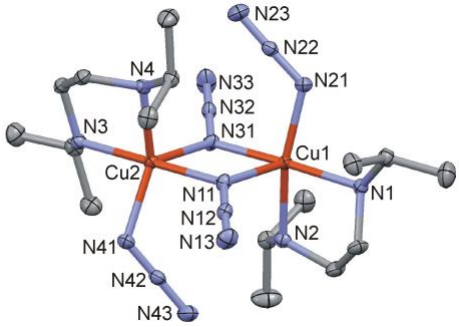

Fig 1. (a) Perspective view of **1**. Symmetry code: (') -x,-y,2-z; and (**b**) Perspective view of **2**.

Table 1. Selected bond distances (Å) and angles (°) for **1**.

Cu(1)-N(1)	2.096(2)	Cu(1)-N(21)	1.991(2)
Cu(1)-N(2)	2.011(2)	Cu(1)-N(11')	2.312(2)
Cu(1)-N(11)	1.995(2)	N(11)-N(12)	1.209(3)
N(12)-N(13)	1.152(3)	N(21)-N(22)	1.189(3)
N(22)-N(23)	1.168(3)		
Cu(1)-N(11)-Cu(1')	101.77(9)	N(2)-Cu(1)-N(11)	174.54(9)
N(1)-Cu(1)-N(21)	146.90(9)	Cu(1)-N(11)-N(12)	125.55(18)
Cu(1')-N(11)-N(12)	125.60(17)	Cu(1)-N(21)-N(22)	128.48(19)
N(13)-N(12)-N(11)	177.1(3)	N(23)-N(22)-N(21)	176.4(3)

Symmetry code: (') -x, -y, 2-z.

$[Cu_2(ip_2en)_2(\mu_{1,1}\text{-}N_3)_2(N_3)_2]$ (2). A perspective view together with the partial atom numbering scheme for the neutral dinuclear complex **2** is presented in Fig. 1(b), and selected bond

parameters are given in Table 2. The copper(II) atoms within the dinuclear unit are bridged by two azide ions in a $\mu_{1,1}$- end-on fashion. The metal centers are penta-coordinated by two N donors of ip$_2$en, N(11) and N(31) atoms of the two azide bridges, and N(21) or N(41) atoms of terminal azide groups. The CuN_5 chromophore around Cu(1) (τ = 0.20) has a slightly distorted SP geometry, whereas Cu(2) (τ = 0.57) can be described as having an intermediate geometry, which is more close to trigonal bipyramid (TBP). The longest Cu-N bond distances are Cu(1)-N(11) = 2.309(3) and Cu(2)-N(31) = 2.274(3) Å whereas the other Cu-N bond lengths vary from 1.979(3) to 2.065(3) Å. The Cu(1)···Cu(2) distance is 3.3526(6) Å and the shortest inter-dinuclear metal-metal separation is 6.6443(8) Å. The Cu(1)-N(11)-Cu(2), Cu(1)-N(31)-Cu(2) bond angles are 101.77(10) and 102.51(10)°. The Cu-N-N bond angles range from 120.0(2) to 134.8(2)°. The "out-of plane" angles are 161.7(3) and 164.8(3)°, respectively. The end-on bridging azide groups are more asymmetric with a mean Δ(N-N) value of 0.066 Å compared to the terminal ones with a mean Δ(N-N) value of 0.030 Å. The N-N-N bond angles of the azide ligands are in the range from 178.1(3) to 179.1(3)°. Hydrogen bonds of type N-H···N link the dinuclear subunits to a supramolecular 2D system oriented along the *a*- and *b*-axis of the unit cell (Table 5, Fig. S2).

Please insert Table 2 close to here

Table 2. Selected bond distances (Å) and angles (°) for **2**.

Cu(1)-N(1)	2.033(3)	Cu(2)-N(3)	2.045(3)
Cu(1)-N(2)	2.065(3)	Cu(2)-N(4)	2.056(3)
Cu(1)-N(11)	2.309(3)	Cu(2)-N(11)	2.004(2)
Cu(1)-N(21)	1.979(3)	Cu(2)-N(31)	2.237(2)
Cu(1)-N(31)	2.020(3)	Cu(2)-N(41)	2.018(2)
N(11)-N(12)	1.211(4)	N(12)-N(13)	1.150(4)
N(21)-N(22)	1.188(4)	N(22)-N(23)	1.162(4)
N(31)-N(32)	1.209(4)	N(32)-N(33)	1.137(4)
N(41)-N(42)	1.196(4)	N(42)-N(43)	1.163(4)
Cu(1)-N(11)-Cu(2)	101.77(10)	Cu(1)-N(31)-Cu(2)	102.51(10)
N(1)-Cu(1)-N(31)	174.21(10)	N(3)-Cu(2)-N(11)	177.28(10)
N(2)-Cu(1)-N(21)	162.16(11)	N(4)-Cu(2)-N(41)	142.83(10)
Cu(1)-N(11)-N(12)	134.8(2)	Cu(2)-N(11)-N(12)	120.3(2)
Cu(1)-N(21)-N(22)	123.0(2)	Cu(2)-N(31)-N(32)	132.8(2)
Cu(1)-N(31)-N(32)	120.0(2)	Cu(2)-N(41)-N(42)	120.0(2)
N(13)-N(12)-N(11)	178.4(3)	N(23)-N(22)-N(21)	178.1(3)
N(33)-N(32)-N(31)	179.1(4)	N(43)-N(42)-N(41)	179.1(3)

***Catena*-[Cu$_2$(Et$_2$Meen)$_2$($\mu_{1,3}$-N$_3$)$_3$]ClO$_4$ (3)**. The structure of **3** consists of an anionic polymeric [Cu$_2$(Et$_2$Meen)$_2$($\mu_{1,3}$-N$_3$)$_3$]$_{nn+}$ chain, which is oriented along the *b*-axis of the unit cell, and perchlorate counter anions. A perspective view together with the partial atom numbering scheme for **3** is given in Fig. 2 and selected bond parameters are presented in Table 3. Each Cu(II) center is penta-coordinated by two N donors of the Et$_2$Meen, and three N atoms of azide ions which generate an alternating sequence of single and double $\mu_{1,3}$-azide bridges within the polymeric chains. The CuN$_5$ chromophores of the two copper atoms have distorted SP geometry with τ-values of 0.22 and 0.26 for Cu(1) and Cu(2), respectively. The apical sites are occupied by N(13') and N(23) atoms [Cu(1)-N(13') = 2.350(3), Cu(2)-N(23) = 2.290(3) Å]. The basal Cu-N bond distances are in the range from 1.983(2) to 2.092(3) Å. The Cu-N-N bond angles vary from 114.8(2) to 136.5(2)°. The N-N bond lengths of the azide groups are in the range from 1.163(4) to 1.191(4) Å, their N-N-N bond angles vary from 174.1(3) to 176.7(3)°. The Cu(1)-N(21)···N(23)-Cu(2), Cu(1)-N(11)···N(13)-Cu(1') and Cu(2)-N(31)…N(33)-Cu(2") torsion angles are -104.1, ±32.2 and ±14.0°, respectively. The intra-chain Cu(1)···Cu(1'), Cu(1)···Cu(2) and Cu(2)···Cu(2") distances are 5.2553(8), 5.4302(8) and 5.0367(8) Å, respectively, and the shortest inter-chain metal-metal separation is 7.5353(10) Å. The eight-membered Cu$_2$(N$_3$)$_2$ rings of the di-$\mu_{1,3}$-azide bridges are located on inversion centers and almost planar ["chair angle θ" which is defined as the acute angle between plane of the di-$\mu_{1,3}$-azide bridges and the N(N$_3$/Cu/N(N$_3$) plane are 17.9° and 7.6°, respectively]. Hydrogen bonds of type N-H···O are formed between N(2) and N(4) donor atoms of ligand Et$_2$Meen to O(1) atoms of the perchlorate ions (Table 5, Fig. S3).

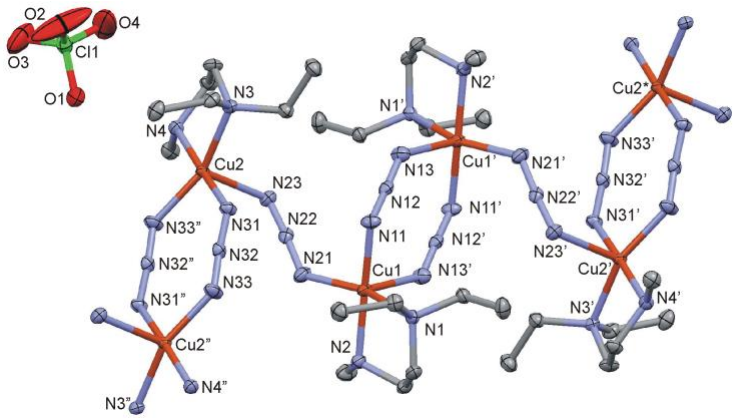

Fig. 2. Perspective view of **3**. Symmetry codes: (') 1-x,1-y,1-z; (") 1-x,-y,1-z; (*) –x,1-y,-z.

Table 3. Selected bond distances (Å) and angles (°) for **3**.

Cu(1)-N(1)	2.092(3)	Cu(2)-N(3)	2.067(2)
Cu(1)-N(2)	2.012(3)	Cu(2)-N(4)	2.006(3)
Cu(1)-N(11)	1.986(3)	Cu(2)-N(31)	1.983(2)
Cu(1)-N(21)	2.003(3)	Cu(2)-N(23)	2.290(3)
Cu(1)-N(13')	2.350(3)	Cu(2)-N(33")	1.996(3)
N(11)-N(12)	1.191(4)	N(12)-N(13)	1.163(4)
N(21)-N(22)	1.189(4)	N(22)-N(23)	1.169(4)
N(31)-N(32)	1.176(4)	N(32)-N(33)	1.174(4)
N(1)-Cu(1)-N(21)	160.57(11)	N(3)-Cu(2)-N(33')	159.14(11)
N(2)-Cu(1)-N(11)	173.85(11)	N(4)-Cu(2)-N(31)	174.59(10)
Cu(1)-N(11)-N(12)	121.3(2)	Cu(2)-N(23)-N(22)	114.8(2)
Cu(1")-N(13)-N(12)	136.5(2)	Cu(2)-N(31)-N(32)	127.4(2)
Cu(1)-N(21)-N(22)	129.2(2)	Cu(2')-N(33)-N(32)	131.4(2)
N(13)-N(12)-N(11)	176.7(3)	N(23)-N(22)-N(21)	176.1(3)
N(33)-N(32)-N(31)	174.1(3)		

Symmetrie codes: (') 1-x, 1-y, 1-z; ('') 1-x, -y, 1-z.

***Catena*-[Cu(ambza)(μ$_{1,1,3}$-N$_3$)$_2$]** (**4**). A perspective view of a section of the structure of **4** together with the partial atom numbering scheme is shown in Fig. 3(a), and selected bond parameters are listed in Table 4. The Cu(1) center is hexa-coordinated by N(1) and N(2) atoms of the ambza chelating ligand, N(21) of a terminal azide group, and N(11), N(11') and N(13") atoms of μ$_{1,1,3}$-briding azide groups. The CuN$_6$ chromophore can be described as an axially elongated tetragonal bipyramid, with N(11') and N(13") in the axial sites [Cu(1)-N(11') = 2.439(3), Cu(1)-N13") = 2.510(3) Å; N(11')-Cu(1)-N(13") = 171.12(10)°]. The equatorial Cu-N bond distances are in the range from 2.010(3) to 2.069(3) Å. Centrosymmetric dinuclear subunits are formed *via* end-on bridging N(11) and N(11') atoms, which in turn are connected to a polymeric 2D system *via* N(13) atoms of the μ$_{1,1,3}$-briding azide groups. The 2D system is oriented along the *b*- and *c*-axis of the unit cell and consists of alternating four atomic Cu$_2$N$_2$ and 16 atomic Cu$_4$(N$_3$)$_4$ rings (Fig. 3(b)). The intra-plane Cu(1)···Cu(1'), Cu(1)···Cu(1$_\#$) and Cu(1')···Cu(1$_\#$) distances are 3.4163(8), 5.6688(11) and 6.8231(12) Å, respectively, and the shortest inter-plane metal-metal separation is 5.1698(10) Å. The Cu(1)-N(11)-Cu(1'), Cu-N(11)-N(12), Cu(1')-N(11)-N(12), N(12)-N(13)-Cu(1$_\#$) and Cu(1)-(N21)-N(22) bond angles are 99.64(12), 127.0(2), 131.4(2), 142.6(2) and 120.4(2)°, respectively. The "out-of plane" angle N(11')···N(11)-N(12) is 167.0(4)°. The Cu(1)-N(11)···N(13)-Cu(1$_\#$) and Cu(1')-N(11)···N(13)-Cu(1$_\#$) torsion angles are -20.8 and 178.7°, respectively. The N-N-N bond

angles of the azide groups are 176.9(3) and 177.6(4)°. Hydrogen bonds of type N-H···N are observed between N(amine) donor atoms of ambza molecules and adjacent azide groups (Table 5, Fig. S4).

Please insert Fig. 3, and Tables 4, 5 close to here

(**a**) (**b**)

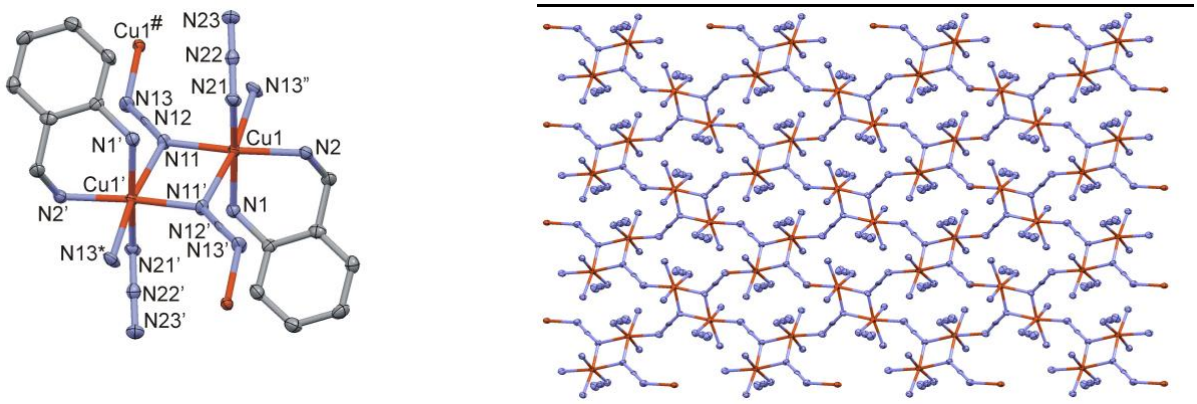

Fig. 3. (a). Perspective view of dinuclear subunit of **4**. Symmetry codes: (‘) –x,1-y,-z; (“) –x,y-1/2,-z+1/2; (#) –x,y+1/2,-z+1/2; (*) x,-y+3/2,z-1/2; **(b)** View onto 2D Cu-azide sublattice of **4**.

Table 4. Selected bond distances (Å) and angles (°) for **4**.

Cu(1)-N(1)	2.069(3)	Cu(1)-N(21)	2.022(3)
Cu(1)-N(2)	2.010(3)	Cu(1)-N(11’)	2.439(3)
Cu(1)-N(11)	2.018(3)	Cu(1)-N(13”)	2.510(3)
N(11)-N(12)	1.196(4)	N(12)-N(13)	1.155(4)
N(21)-N(22)	1.212(4)	N(22)-N(23)	1.155(4)
Cu(1)-N(11)-Cu(1’)	99.64(12)	N(2)-Cu(1)-N(11)	171.19(12)
N(1)-Cu(1)-N(21)	169.66(12)	N(11’)-Cu(1)-N(13”)	171.12(10)
Cu(1)-N(11)-N(12)	127.0(2)	Cu(1)-N(21)-N(22)	120.4(2)
Cu(1’)-N(11)-N(12)	131.4(2)	N(23)-N(22)-N(21)	177.6(4)
N(13)-N(12)-N(11)	176.9(3)		

Symmetry code: (‘) -x, 1-y, -z; (“) –x, y-1/2, -z+1/2.

Table 5. Hydrogen bond systems for compounds **1** – **4**.

D-H…A[a]	Symmetry of A	D…A (Å)	D-H…A (°)
Compound **1**			
Cu(1)-H(91)…N(23)	[-x,1-y,2-z]	3.033(4)	165(3)
Compound **2**			
N(1)-H(91)…N(43)	[3/2-x,1/2+y,1/2-z]	3.104(4)	170(3)
N(2)-H(92)…N(43)		3.182(4)	165(3)
N(3)-H(93)…N(23)	[5/2-x,-1/2+y,1/2-z]	3.034(4)	164(3)
N(4)-H(94)…N(23)		3.223(4)	150(3)
Compound **3**			
N(2)-H(91)…O(1)	[1-x,1-y,1-z]	3.131(4)	153(3)
N(4)-H(92)…O(1)		3.067(4)	168(4)
Compound **4**			
N(1)-H(90)…N(23)	[-x,1/2+y,1/2-z]	3.186(5)	153(3)
N(1)-H(91)…N(21)	[-x,1-y,-z]	3.184(4)	164(3)
N(2)-H(92)…N(21)	[-x,-y,-z]	3.058(4)	175(3)
N(2)-H(93)…N(13)	[x,-1+y,z]	3.100(5)	166(3)

[a] D = Donor, A = Acceptor

Magnetic properties

For the dinuclear compound $[Cu_2(Et_3en)_2(\mu_{1,1}\text{-}N_3)_2(N_3)_2]$ (**1**) the $\chi_M T$ value at room temperature (0.89 $cm^3mol^{-1}K$, Fig. 4) decreases slowly as the temperature decreases until ~25 K and then after a rapid decrease was observed reaching a value of 0.53 $cm^3mol^{-1}K$ at 2 K, indicating an antiferromagnetic coupling. The χ_M *vs* T plot provides more information about this magnetic behavior: the χ_M value of 2.97 x 10^{-3} cm^3mol^{-1} at room temperature increases as the temperature decreases reaching a maximum of 0.26 cm^3mol^{-1} at 2 K. This behavior clearly indicates a weak antiferromagnetic coupling. Based on this situation, the experimental magnetic data have been fitted using the expression (Eq. 1) derived through the Hamiltonian $\hat{H} = -J\hat{S}_A.\hat{S}_B$ with $S_A = S_B = ½$

$$\chi_M = (2N\, g^2\mu_B^2/kT)[(\exp(J/kT))/(1+3\exp(J/kT)] \quad (1)$$

The parameters N, μ_B and k in Eq 1 have their usual meanings. Least-squares fitting of all experimental data led to $J = -1.8$ cm^{-1} and g = 2.17.

Taking into consideration that **1** is a dinuclear compound which shows the bridging azide ions $\mu_{1,1}$ (end-on, EO) coordination mode forming a $[Cu_2(\mu_{1,1}\text{-}N_3)_2]$ central rectangle with Cu(1)-

N(11) and Cu(1)-N(11') distances of 1.995 and 2.312 Å, respectively. This is a basal–apical disposition of the bridging Cu-N distances on the central [$Cu_2(\mu_{1,1}\text{-}N_3)_2$] core.[14,57-60] Usually, this basal–apical geometry gives rise very small magnetic couplings since the magnetic orbital containing the unpaired electron is mainly of an $d_{x^2-y^2}$ type lying in the basal plane of the copper atoms with an almost negligible contribution on the axis perpendicular to the basal plane. For such small coupling, the Cu–N–Cu angle is not indicative of the magnetic interaction.[60]

Please insert Fig. 4 close to here

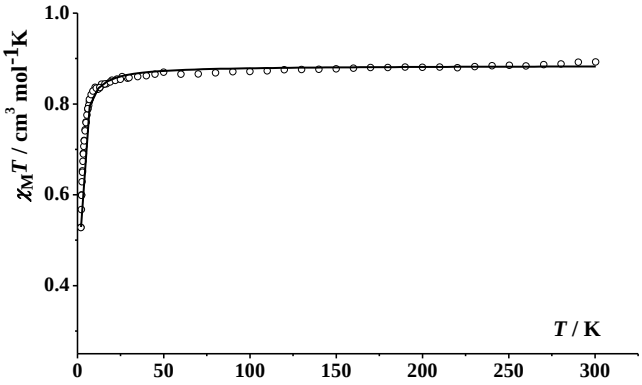

Fig. 4. Plot of the observed $\chi_M T$ *vs* T of compound **1**. Solid line represents the best fit (see text).

On the other hand, in the dinuclear compound [$Cu_2(ip_2en)_2(\mu_{1,1}\text{-}N_3)_2(N_3)_2$] (**2**) the $\chi_M T$ value at room temperature (0.88 $cm_3mol_{-1}K$, Fig. 5) increases as the temperature decreases arriving to a maximum of 1.08 $cm_3mol_{-1}K$ at 6 K and then decreases rapidly to a value of 0.99 $cm_3mol_{-1}K$ at 2 K. This behavior indicates a weak ferromagnetic coupling. Based on this situation, the experimental magnetic data have been fitted in the interval 6-300 K using the same expression (Eq. 1) shown above for complex **1**. Least-squares fitting of all experimental data resulted in J = 7.0 cm_{-1} and g = 2.15.

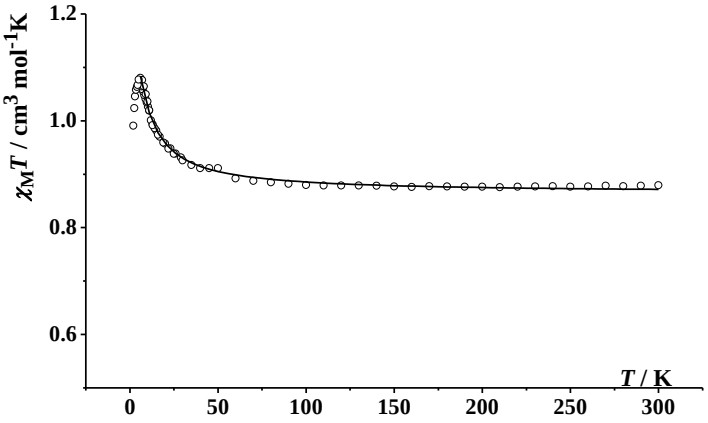

Fig. 5. Plot of the observed $\chi_M T$ *vs* T of compound **2**. Solid line represents the best theoretical fit (see text).

As in the case of **1**, compound **2** is a dinuclear compound which shows the $\mu_{1,1}$ (end-on, EO) coordination mode with the bridging azide ions forming a $[Cu_2(\mu_{1,1}\text{-}N_3)_2]$ central rectangle, where Cu(1)-N(11) and Cu(1)-N(11') distances are 2.004, 2.020 and 2.310, 2.273 Å, respectively (basal–apical disposition of the bridging Cu-N distances on the central $[Cu_2(\mu_{1,1}\text{-}N_3)_2]$ core.[14,57-60] The structural parameters of **1** and **2,** which are collected in Table 6, are similar and the difference was found in the Addison parameters for the copper atoms: **1** is centrosymmetric with $\tau = 0.46$ (almost intermediate geometry between SP and TBP), whereas $\tau = 0.57$ and 0.20 for the copper atoms in **2** (TBP geometry is slightly dominating around Cu1 and distorted SP for Cu2). Probably, this difference in the geometries around the Cu(II) centers may tentatively explain the different observed magnetic behavior in the two compounds.

Table 6. Structural parameters and singlet-triplet coupling constants in compounds **1** and **2**.

Compound	Cu-($\mu_{1,1}$-N)ap (Å)	Cu-($\mu_{1,1}$-N)basal (Å)	angle (°)	τCu(1)	τCu(2)	J (cm^{-1})
1	2.312	1.994	101.78	0.46	0.46	-1.8
2	2.310, 2.273	2.004, 2.020	101.77, 102.53	0.57	0.20	7.07

A plot of the molar magnetic susceptibility (for two copper atoms) *vs. T* for *catena*-$[Cu_2(Et_2Meen)_2(\mu_{1,3}\text{-}N_3)_3]ClO_4$ (**3**) is shown in Fig 6. The χ_M value per two copper atoms is 1.6×10^{-3} cm^{3}mol^{-1} at room temperature. It increases with decreasing the temperature reaching a maximum value of 7.7 x 10^{-3} cm^{3}mol^{-1} at 30 K, then decreases to a minimum value of 1.2 x 10^{-3}

cm3mol-1 at 5 K followed by a further increase to 1.85 x 10-3 cm3mol-1 at 2 K due to the presence of a small quantity of paramagnetic impurities.

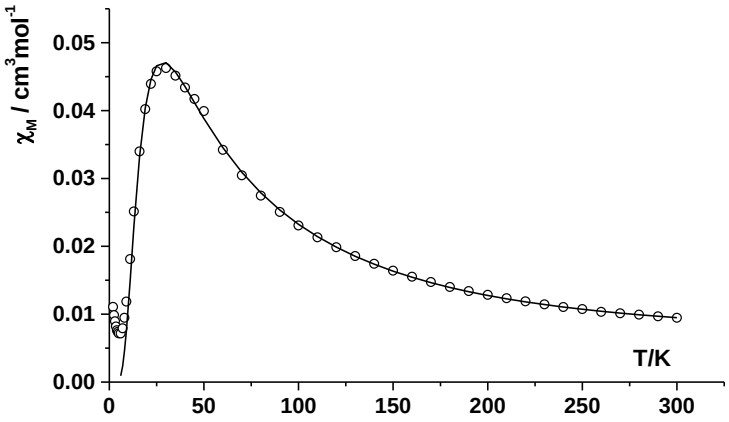

Fig. 6. Plot of the observed χ_M *vs* T of compound **3**. Solid line represents the best theoretical fit (see text).

Compound **3** shows a topology for Cu(II) which is different from the previous two compounds: an alternating chain [Cu(1)($\mu_{1,3}$–N_3)$_2$Cu(1')]-($\mu_{1,3}$–N_3)-[Cu(2')($\mu_{1,3}$–N_3)$_2$Cu(2'')]-($\mu_{1,3}$–N_3)-[Cu(1)($\mu_{1,3}$–N_3)$_2$Cu(1')]-… with different structural parameters in the dinuclear entities [Cu(1)($\mu_{1,3}$–N_3)$_2$Cu(1')] and [Cu(2")($\mu_{1,3}$–N_3)$_2$Cu(2)]. Accordingly, three different coupling constants J_1-J_2-J_3-J_2-J_1-J_2-J_3…. should theoretically be present in the alternating chain but unfortunately, as far as we know, such analytical expression was not established yet. As an approach to the *J* coupling constants, a fit based on the interaction Scheme 1 was performed by means of the computer program PHI using the Hamiltonian:[61]

$$H = -J_1(S_1S_2 + S_5S_6 + S_9S_{10}) - J_2(S_2S_3 + S_4S_5 + S_6S_7 + S_8S_9 + S_{10}S_{11} + S_{12}S_1) - J_3(S_3S_4 + S_7S_8 + S_{11}S_{12}) \quad (2)$$

Taking into consideration the fact which was already reported in the literature that a 12-membered ring of S = ½ describes satisfactorily the magnetic behavior of the chain. The best fit parameters were $J_1 = -31.1$ cm^{-1}, $J_2 = 4.1$ cm^{-1}, $J_3 = -802.6$ cm^{-1} and g = 2.15. However, it is worth noting that the shape of the fitted curve (Fig. 6) does not change over a wide range of J_3 values. For J_3 values more antiferromagnetic than –500 cm-1 the susceptibility curves remain unchanged. Thus, the fitting procedure cannot provide an accurate value for such exchange interaction. The analysis of the structure indicates that such interaction corresponds to doubly bridged azido [Cu($\mu_{1,3}$–N_3)$_2$Cu]

moiety with four short Cu-N distances. The Cambridge Structural Database search indicates that such moiety is only present in two compounds, TTZZCU10 and DUCGEN refcodes,[62,63] and in the latter case an antiferromagnetic interaction with a *J* value of more than -800 cm^{-1} was reported. DFT calculations for such system gives a *J* value -1270 cm^{-1}.[64] However, there are many examples in the literature of $[Cu(\mu_{1,3}–N_3)_2Cu]$ moieties but usually with two long and two short Cu-N distances.

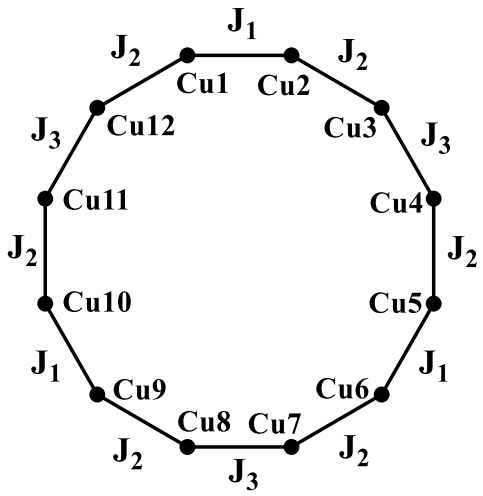

Scheme 1. Schematic diagram representing the exchange interactions within a ring of 12 Cu atoms (S = ½) for complex **3**.

For *catena*-$[Cu(ambza)(\mu_{1,1,3}\text{-}N_3)_2]$ (**4**) the $\chi_M T$ value at room temperature (0.88 $cm^3mol^{-1}K$) increases as the temperature decreases (Fig. 7) reaching a maximum value of 1.08 $cm^3mol^{-1}K$ at 7 K and then after it decreases to 0.71 $cm^3mol^{-1}K$ at 2 K. This behavior indicates a bulk ferromagnetic coupling. From the structural point of view, complex **4** is a 2D system in which each $[Cu_2(\mu_{1,1}\text{-}N_3)_2]^{2+}$ dinuclear subunit is connected to four similar dinuclear subunits *via* the N(13) atoms of the $\mu_{1,1,3}$-briding azide groups. The Cu(1)-N(13") distance is long (2.510 Å) and to the first approximation we can consider complex **4** as formed by "isolated" $[Cu_2(\mu_{1,1}\text{-}N_3)_2]^{2+}$ units. Based on this situation, the experimental magnetic data between 300 and 7 K have been fitted using the same expression (Eq. 1) which was derived through the Hamiltonian $\hat{H} = -J\hat{S}_A.\hat{S}_B$ with $S_A = S_B = ½$ for complex **1**. Least-squares fitting of all experimental data led to *J* = 7.7 cm^{-1} and g = 2.15.

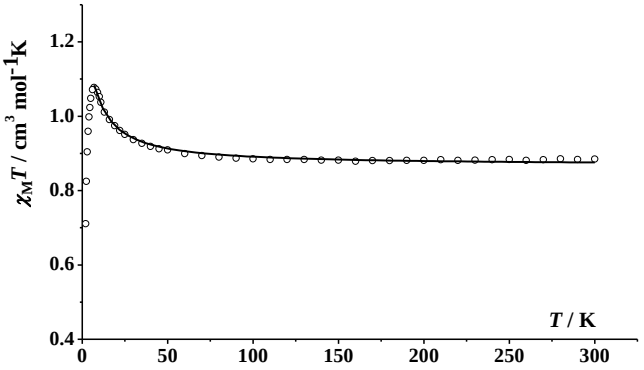

Fig. 7. Plot of the observed $\chi_M T$ *vs* T of compound **4**. Solid line represents the best theoretical fit (see text).

DFT Study of exchange interactions in the chain compound 3

The exchange interactions in the chain compound **3** were performed with Density Functional Theory[65] calculations using the Siesta code.[66,67] For such calculations, the PBE+U approach[68,69] was employed because it provides a better agreement with the experimental exchange coupling constants than the pure functionals. Only valence electrons are included in the calculations, with the core being replaced by norm-conserving scalar relativistic pseudopotentials factorized in the Kleinman−Bylander form.[70] The pseudo potentials are generated according to the method proposed by Trouiller and Martins.[71] As basis set, a double-ζ with polarization was employed for all the atoms. There are two key parameters that control the accuracy of the numerical calculations in Siesta: (i) because the wave function vanishes at the chosen confinement radius r_C, whose value is different for each atomic orbital, the energy radii of different orbitals is determined by a single parameter, the energy shift, which is the energy increase of the atomic eigenstate due to the confinement and (ii) the integrals of the self-consistent terms are obtained with the help of a regular real space grid in which the electron density is projected. The grid spacing is determined by the maximum kinetic energy of the plane waves that can be represented in that grid. We have employed in the calculations an energy shift of 50 meV and maximum kinetic energy value of 250 Ry; with such values we have a convergence in the results.[72,73] The *J* values were calculated using five spin configurations, the high spin case with the four atoms of the unit cell with a parallel alignment and other four S =1

calculations with the spin inversion of one center.[74] The calculated values are $J_1 = -11.9$ cm^{-1}, $J_2 =$ 3.8 cm^{-1}, $J_3 = -1391.7$ cm^{-1}. Comparison of the calculated values with the fitted data ($J_1 = -31.1$ cm^{-1}, $J_2 = 4.1$ cm^{-1}, $J_3 = -802.6$ cm^{-1}) indicates that the calculated J_1 value is slightly smaller than the fitted J_1 value but the calculations reproduce qualitative the exchange interactions. Such exchange coupling constant corresponds to a double 1,3-azido bridging ligand with two short Cu-N distance (Fig. 8). The presence of one long Cu-N distance in the two bridging ligand results in a weak antiferromagnetic coupling.

Quantum Monte Carlo simulations were performed to compare the susceptibility curves obtained using the finite-model fitted and DFT calculated sets of *J* values with the experimental data (see Fig. 9). Thus, using the set of calculated DFT *J* values results in quantitative disagreement due to the small J_1 value that provides a discrepancy below 30 K because such J_1 value (-11.9 cm^{-1}) is too small and the curve starts to decay at very low temperatures. The set of *J* values fitted with a 12-atoms ring model improves the results with a larger J_1 value (-31.1 cm^{-1}) the curve drops down at higher temperatures. However, the curve still remains slightly different than the experimental one showing the limitations of a fitting procedure using a finite model to simulate a chain structure. Finally, keeping all the fitted values but increasing J_1 until -42.6 cm^{-1} a relatively good agreement with the experimental curve is found. Probably, we should comment on the difference of the J_3 exchange coupling, in such case with four short Cu-N distances there is a huge strengthening of the antiferromagnetic interactions. Concerning the J_3 value, we have already mentioned that values more antiferromagnetic than -500 cm^{-1} fit the experimental curve without any change. Also, the comparison with the unique reported system (CSD refcode DUCGEN)[63] which is a dinuclear complex with a double 1,3-azido bridging ligand with four short Cu-N distances shows a nice agreement with the value of -1270 cm^{-1} calculated with the hybrid B3LYP functional.[64] This functional provides quite accurate exchange coupling constant values for Cu^{II} dinuclear complexes, and such value is also in agreement with the proposed experimental value < -800 cm^{-1} due to the impossibility to fit the curve. Finally, in the unit cell there are two almost identical interactions (J_2 constant) with a single 1,3-azido ligand also with one long Cu-N distance. Such exchange pathway is quite uncommon not only for the coordination mode but also for the relative position of the Cu^{II} cations. Thus, considering the terminal nitrogen atoms of the azido ligand, the Cu-N$_{term}$-N$_{term}$-Cu torsion angle is 105º being in an intermediate position with respect to the most common *cis* and *trans* bridging modes with (0 and 180º torsion angle values).[75] The presence of a long Cu-N distance

makes the orbital bearing the unpaired electron of this Cuii center is perpendicular to the exchange pathway resulting in a negligible overlap with the second Cuii center (that is related with the antiferromagnetic contribution) resulting in a predominant ferromagnetic contribution.

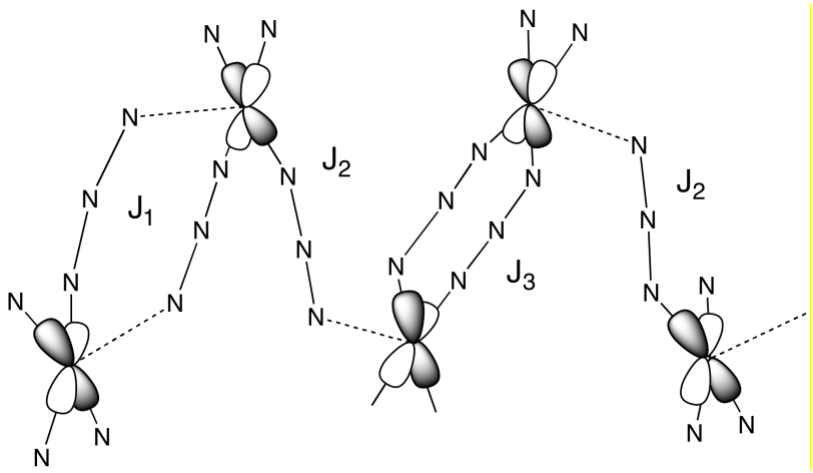

Fig. 8. Description of the exchange interaction pathways and orientation of the orbitals with the unpaired electrons of the chain in compound **3**. Long Cu-N distances are indicated with dashed lines.

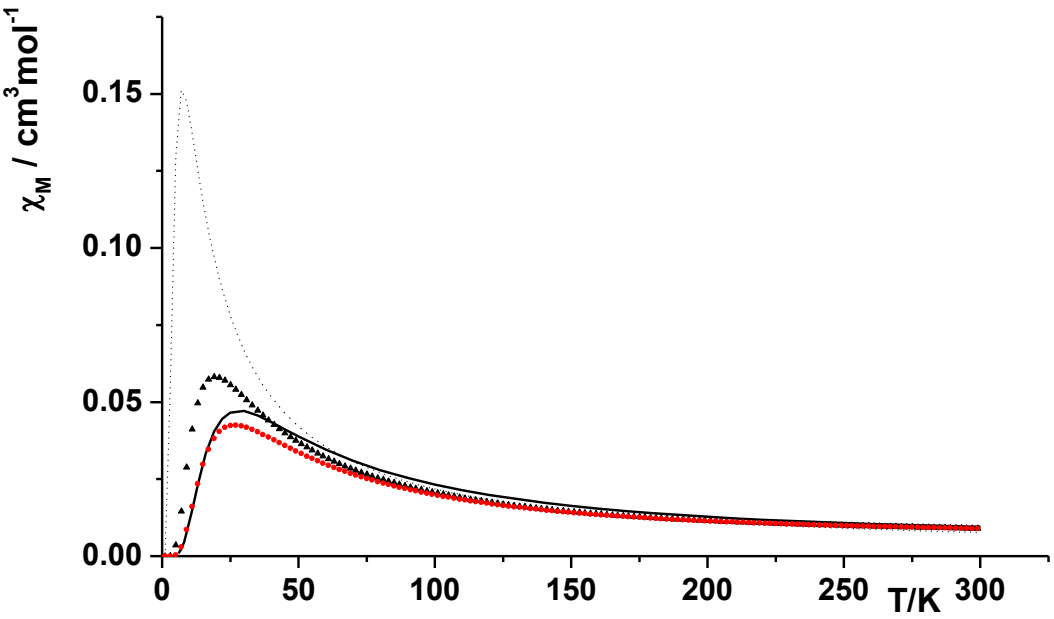

Fig. 9. Solid black line corresponds to the experimental data. The other three curves were obtained by performing quantum Monte Carlo simulations, dotted line correspond to the set of *J* values obtained with DFT calculations, black triangles with the values optimized using fhi code and a 12-atoms ring model and the red circles is the same optimized set but increasing the J_1 value from -31.1 to -42.6 cm^{-1}.

Experimental

Materials and physical measurements

N,N,N`*-Triethyl-1,2-diaminoethane, *N,N`-diisopropyl-1,2-diaminoethane, *N,N*-diethyl-*N`*-methyl-1,2-diaminoethane and 2-aminobenzylamine were purchased from TCI-America. All other materials were reagent grade quality. Infrared spectra were recorded on JASCO FT/IR-480 plus spectrometer as KBr pellets. Electronic spectra were recorded using Agilent 8453 HP diode UV-VIS. spectrophotometer. The molar conductivity of a solution sample was determined from $\Lambda_M = (1.0 \times 10^3 \kappa)/[Cu]$, where κ = specific conductance and [Cu] is the molar concentration of the complex. The measurements were performed using Mettler Toledo Seven Easy conductometer and calibration was determined by the aid of 1413 μS/cm conductivity standard. Elemental analyses were carried out by the Atlantic Microlaboratory, Norcross, Georgia U.S.A. Variable-temperature magnetic studies were performed in the Magnetochemistry Service of the University of Barcelona using a DSM5 Quantum Design magnetometer operating at 1 T in the 300-2.0 K range. Diamagnetic corrections were applied to the observed paramagnetic susceptibility using Pascal's constants.

Synthesis of the complexes

Caution*! Salts of perchlorate and azide as well as their metal complexes are potentially explosive and should be handled with great care and in small quantities.*

$[Cu_2(Et_3en)_2(\mu_{1,1}\text{-}N_3)_2(N_3)_2]$ (1). A mixture of copper(II) perchlorate hexahydrate (0.190 g, 0.50 mmol) and *N,N,N`*-triethyl-1,2-diaminoethane (0.073 g, 0.5 mmol) were dissolved in 20 ml MeOH. To this mixture an aqueous solution of sodium azide (0.065 g, 1.0 mmol) dissolved in H_2O (3 mL) was added dropwise. The solution was heated on a steam-bath for 3 min, filtered through celite and the resulting intense green solution was allowed to crystallize at room temperature. In the following day, the dark green well shaped crystals which separated were collected by filtration, washed with propan-2-ol, ether and then air dried (overall yield: 110 mg, 75%). Characterization:

Elemental analysis: Anal. calcd for $C_{16}H_{40}Cu_2N_{16}$ (583.99 g/mol): C, 32.91; H, 6.87; N, 38.38%. Found: C, 33.19; H, 3.66; N, 38.40 %. Selected IR bands (cm^{-1}): 3158 (w) ν(NH); 2963 (w) ν(CH); 2055 (vs), 2036 (vs) $\nu(N_3)$. UV-VIS spectrum {λ_{max}, nm (ε_{max} per Cu atom, $M^{-1}cm^{-1}$)} in CH_3CN: ~ 600 (479, br). Λ_M (CH_3CN) = 5.2 $\Omega^{-1}cm^2mol^{-1}$.

$[Cu_2(ip_2en)_2(\mu_{1,1}\text{-}N_3)_2(N_3)_2]$ (**2**). Copper(II) nitrate trihydrate (0.122 g, 0.50 mmol) and *N*,*N*`-diisopropyl-1,2-diaminoethane (0.072 g, 0.5 mmol) were dissolved in 20 ml MeOH. To this mixture an aqueous solution of sodium azide (0.065 g, 1.0 mmol in 3 mL H_2O) was added dropwise. The solution was heated on a steam-bath for 3 min, filtered through celite and intense green solution was allowed to crystallize at room temperature. In the following day, the light olive-green crystalline compound which separated was collected by filtration, washed with propan-2-ol, ether and then air dried (overall yield: 97 mg, 66%). Well-shaped crystals of X-ray quality were obtained from dilute solutions. Characterization: Elemental analysis: Anal. calcd for $C_{16}H_{40}Cu_2N_{16}$ (583.99 g/mol): C, 32.91; H, 6.87; N, 38.38%. Found: C, 32.73; H, 6.74; N, 38.07%. Selected IR bands (cm^{-1}): 3196 (m) ν(NH); 2969 (m) (CH); 2094 (s), 2034 (vs), 2028 (vs) $\nu(N_3)$. Visible spectrum {λ_{max}, nm (ε_{max}, $M^{-1}cm^{-1}$/Cu atom)} in CH_3CN: 626 (359). Λ_M (CH_3CN) = 2.8 $\Omega^{-1}cm^2mol^{-1}$.

***Catena*-$[Cu_2(Et_2Meen)_2(\mu_{1,3}\text{-}N_3)_3]ClO_4$ (3).** The complex was isolated as dark green crystals using a procedure similar to that described above for complex **1** except *N*,*N*-diethyl-*N*`-methyl-1,2-diaminoethane was used instead of *N*,*N*`-diisopropyl-1,2-diaminoethane (overall yield: 72%). Single crystals suitable for X-Ray were obtained from dilute solutions. Characterization: Elemental analysis: Anal. calcd for $C_{33}H_{40}N_{12}Cl_2Cu_2O_{10}$ (613.07 g/mol): C, 27.43; H, 5.92; N, 29.70%. Found: C, 27.66; H, 5.84; N, 29.94%. Selected IR bands (cm^{-1}): 3235 (w) ν(NH); 2970 (w), 2928 (w) ν(CH); 2104 (vs), 2057 (s), 2026 (vs) $\nu(N_3)$; 1120 (s), 1081 (m) ν(Cl-O) (ClO_4^-). UV-VIS spectrum {λ_{max}, nm (ε_{max}, $M^{-1}cm^{-1}$/Cu atom)} in CH_3CN: 609 (347). Λ_M (CH_3CN) = 174 $\Omega^{-1}cm^2mol^{-1}$.

***Catena*-$[Cu(ambza)(\mu_{1,1,3}\text{-}N_3)_2]$ (4).** The complex was synthesized using a similar procedure as that described for complex **2**, except 2-aminobenzylamine ligand was used instead of *N*,*N*`-diisopropyl-1,2-diaminoethane. Single green crystals suitable for X-ray structure determination were obtained from dilute solution (overall yield: 65%). Characterization: Elemental analysis: Anal. calcd for $C_7H_{10}N_8Cu$ (molar mass = 269.76 g/mol): C, 31.17; H, 3.74; N, 41.54%. Found: C, 31.29; H, 3.36; N, 41.55%. Selected IR bands (cm^{-1}): 3246 (m), 3202 (m) ν(NH) (NH_2); 3115 (m), 2944

(vw), 2891 (w) ν(CH); 2062 (vs), 2030 (vs), 2016 (s) ν(N_3). UV-VIS spectrum {λ_{max}, nm (saturated)} in CH_3CN: 272, 390, 569 (sh), 638 nm.

X-ray crystal structure analysis

The X-ray single-crystal data of the four compounds were collected on a Bruker-AXS APEX-II CCD diffractometer at 100(2) K. The crystallographic data, conditions retained for the intensity data collection and some features of the structure refinements are listed in Table 7. The intensities were collected with Mo-Kα radiation (λ= 0.71073 Å). Data processing, Lorentz-polarization and absorption corrections were performed using SAINT, APEX and the SADABS computer programs.[76] The structures were solved by direct methods and refined by full-matrix least-squares methods on F_2, using the SHELXL program suite.[77] All non-hydrogen atoms were refined anisotropically. The hydrogen atoms were located from difference Fourier maps, assigned with isotropic displacement factors and included in the final refinement cycles by use of geometrical constraints. Molecular plots were performed with the Mercury program.[78]

Table 7. Crystallographic data and processing parameters for compounds **1** – **4**.

Compound	**1 (#2742)**	**2 (#2744)**	**3 (#2743)**	**4 (#2915)**
Empirical formula	$C_{16}H_{40}Cu_2N_{16}$	$C_{16}H_{40}Cu_2N_{16}$	$C_{14}H_{36}ClCu_2N_{13}O_4$	$C_7H_{10}CuN_8$
Formula mass	583.74	583.74	613.11	269.78
System	Triclinic	Monoclinic	Triclinic	Monoclinic
Space group	P-1	$P2_1/n$	P-1	$P2_1/c$
a (Å)	8.5860(10)	11.8730(10)	7.8921(9)	12.3260(14)
b (Å)	8.6070(10)	12.0334(11)	12.8529(12)	6.8100(10)
c (Å)	9.1858(12)	19.5852(14)	13.2899(14)	13.4660(16)
α (°)	85.110(14)	90	70.941(13)	90
β (°)	84.700(13)	107.191(9)	82.294(14)	117.036(3)
γ (°)	78.652(16)	90	82.146(14)	90
V ($Å^3$)	661.15(14)	2673.2(4)	1256.5(3)	1006.8(2)
Z	1	4	2	4
T (K)	100(2)	100(2)	100(2)	100(2)
μ (mm^{-1})	1.646	1.628	1.847	2.155
D_{calc} (Mg/m^3)	1.466	1.450	1.620	1.780
Crystal size (mm)	0.24x0.22x0.11	0.44x0.36x0.25	0.44x0.35x0.15	0.32x0.16x0.08
θ max (°)	26.27	26.33	26.34	26.00
Data collected	4167	18282	10079	7340
Unique refl. / R_{int}	2484 / 0.0215	5343 / 0.0385	5039 / 0.0183	1988 / 0.0531
Parameters / Restraints	160 / 1	327 / 4	319 / 2	157 / 4
Goodness-of-Fit on F^2	1.058	1.115	1.024	1.117
R1 / wR2 (all data)	0.0355 / 0.0958	0.0407 / 0.0950	0.0406 / 0.1072	0.0457 / 0.1034
Residual extrema ($e/Å^3$)	1.07 / -0.65	0.78 / -0.39	1.80 / -0.91	0.77 / -0.53

Quantum Monte Carlo simulations

It is well-known, the limitation of the exact diagonalization approach to handle with periodic systems. Thus, Quantum Monte Carlo methods represent a good alternative way to verify the accuracy of the ring model employed in the fitting with the phi program. Quantum Monte Carlo simulations for a 1D chain system were based on the directed loop algorithm method developed by Sandvik et al.[79] QMC1 were carried out using the ALPS 2.0 library (dirloop_see

method).QMC2,QMC3[80,81] For the susceptibility dependence with the temperature, usually we employ 108 steps for the simulations between 2 and 300 K and a whole simulation must be performed at each temperature. The initial 10% of steps was employed for thermalization of the system in all calculations.

Conclusions

Here we have presented four new compounds with azido as the bridging ligand synthesized from the S = 1/2 Cu(II) cation and a terminal L ligand. The new compounds are: [Cu2(Et3en)2(μ1,1-N3)2(N3)2] (1), [Cu2(ip2en)2(μ1,1-N3)2(N3)2] (2), catena-[Cu2(Et2Meen)2(μ1,3-N3)3]ClO4 (3) and catena-[Cu(ambza)(μ1,1,3-N3)2] (4), where Et3en = N,N,N`-triethyl-1,2-diaminoethane; ip2en = N,N`-diisopropyl-1,2-diaminoethane; Et2Meen = N,N-diethyl-N`-methyl-1,2-diaminoethane; ambza = 2-aminobenzylamine. Compounds **1–4** are representative of the great diversity of dimensionalities and topologies found in the Cu(II)-azido bridging compounds: **1** and **2** are dinuclear compounds with doubly bridged $\mu_{1,1}$-N3, whereas **3** and **4** complexes consitute polymeric species with alternative sequence of single and double μ1,3-N3 bridges for 3 with 1D chain, and triple $\mu_{1,1,3}$-briding azide in **4** with 2D extended structure. Compound **3** shows a new topology for Cu(II) alternating chains $[Cu(1)(\mu_{1,3}–N_3)_2Cu(1')]$-$(\mu_{1,3}–N_3)$-$[Cu(2')(\mu_{1,3}–N_3)_2Cu(2'')]$-$(\mu_{1,3}–N_3)$-$[Cu(1)(\mu_{1,3}–N_3)_2Cu(1')]$-…. . Variable temperature magnetic susceptibility over the temperature range 2-298 K revealed weak antiferromagnetic coupling (J = -1.8 cm-1) for **1**, and ferromagnetic coupling with J values of 7.0 and 7.7 cm-1, respectively for complexes **2** and **4**, respectively. The three different coupling constants for **3** have been obtained through fitting procedure assuming a ring-model and by DFT calculations. The Cu-N distances play a fundamental role to determine the sign and magnitude of the exchange coupling interactions. Thus, there is an unusual double 1,3-N_3 azido bridging ligand with four short Cu-N distances (J_3) showing a very strong antiferromagnetic coupling. However, also for a double 1,3-N_3 azido bridge the presence of one long Cu-N distances in each exchange pathway results in a moderate antiferromagnetic coupling (J_1). This value is the most significant parameter to control the shape of the susceptibility curves below 50 K. Despite the large antiferromagnetic J_3 value (−1391.7 and −802.6 cm^{-1} DFT and fitted values, respectively) a large change in J_3 does not affect the susceptibility curve. Finally, the third exchange interaction (J_2) corresponds to a single 1,3-N_3 azido bridging ligand with one long Cu-N distance leading to a small ferromagnetic coupling. It is worth mentioning the nice agreement between DFT and fitted experimental values being the discrepancy in the J_1 value (−11.9 and −31.1 DFT and fitted values, respectively) the origin of the differences in the susceptibility curves.

Acknowledgments

S. S. M. acknowledges the financial support of this research by the Department of Chemistry-University of Louisiana at Lafayette and by the Spanish *Ministerio de Economía y Competitividad* (grants CTQ2015-64579-C3-1-P and CTQ2015-63614-P, MINECO/FEDER, UE). E.R. thanks Generalitat de Catalunya for an ICREA Academia award. E.R. thankfully acknowledges the computer resources in the Consorci Serveis Universitaris de Catalunya (CSUC). L.M. thanks Conicyt-Chile for a predoctoral fellowship.

Appendix A. Supplementary material

CCDC 1555779-1555782 contain the supplementary crystallographic data for **1** - **4**, respectively. These data can be obtained free of charge from The Cambridge Crystallographic Data Centre via www.ccdc.cam.ac.uk/data_request/cif. Supplementary data associated with this article (Packing plots of complexes **1-4** are given in Figs S1-S4, respectively) can be found, in the online version at doi:10.1016/???

References

1. T. S. Lin and W. H. Prusoff, *J. Med. Chem.*, 1978, **21**, 109-112.
2. (a) S. Piantadosi, C. J. Marasco and E. J. Modest, *J. Med. Chem.*, 1991, **34**, 1408-1414; (b) T. Pathak, Chem. Rev. 2002, **102**, 1623-1668.
3. S. Bräse, C. Gil, K. Knepper and V. Zimmermann, *Angew. Chem. Int. Ed.*, 2005, **44**, 5188-5240.
4. H. H. Jobelius and H.-D. Scharff "Hydrazoic Acid and Azides" in Ullmann's Encyclopedia of Industrial Chemistry, 2005, Wiley-VCH, Weinheim. doi:10.1002/14356007.a13_193
5. (a) E. I. Solomon, U. M. Sundrama and T.E. Machonkin, *Chem. Rev.*, 1996, **96**, 2563-2606; (b) E. I. Solomon, M. J. Baldwin and M. D. Lowery, *Chem. Rev.*, 1992, **92**, 521-542; (c) K. D. Karlin and Z. Tyeklár (Eds), Bioinorganic Chemistry of Copper, Chapman & Hall, New York, 1993.
6. (a) F. A. Mautner, F. R. Louka, J. Hofer, M. Spell, A. Lefèvre, A. E. Guilbeau and S. S. Massoud, *Cryst. Growth Des.*, 2013, **13**, 4518-4525; (b) F. A. Mautner, C. Berger, M. J. Dartez, Q. L. Nguyen, J. Favreau, S. S. Massoud, *Polyhedron*, 2014, **69**, 48-54; (c) F. A. Mautner, M. Scherzer, C. Berger, R. C. Fischer and S. S. Massoud, *Inorg. Chim. Acta*, 2015, **425**, 46-51.
7. (a) B. Machura, I. Nawrot, R. Kruszynski and M. Dulski, *Polyhedron*, 2013, **54**, 272-284; (b) B. Machura, I. Nawrot and K. Michalik, Polyhedron, 2012, **31**, 548-557; (c) B. Machura, A. Świtlicka, I. Nawrot, J. Mroziński and K. Michalik, *Polyhedron*, 2011, **30**, 2815-2823.
8. (a) S. S. Massoud, F. R. Louka, Y. K. Obaid, R. Vicente, J. Ribas, R. C. Fischer and F. A. Mautner, *Dalton Trans.*, 2013, **24**, 3968-3978; (b) F. A. Mautner, M. Koikawa, M. Mikuriya, E. H. Harrelson and S. S. Massoud, *Polyhedron*, 2013, **59**, 17-23; (c) M. A. M. Abu Youssef, A. Escuer, F. A. Mautner and L. Öhrström, *Dalton Trans.*, 2008, 3553-3558.
9. (a) A. Escuer, M. Font-Bardia, S. S. Massoud, F. A. Mautner, E. Penalba, X. Solans and R. Vicente, *New J. Chem.*, 2004, **28**, 681-686; (b) S. S. Massoud and F. A. Mautner, *Inorg. Chim. Acta*, 2005, **358**, 3334-3340.
10. (a) S. S. Massoud, F. A. Mautner, R. Vicente A. A. Gallo and E. Ducasse, *Eur. J. Inorg. Chem.*, 2007, 1091-1102; (b) F. A. Mautner, M. Scherzer, C. Berger, R.C. Fischer, R. Vicente and S. S Massoud, *Polyhedron*, 2015, **85**, 329-336.
11. S. Ray, S. Koner, A. Jana, A. Dhara, K. Das, S. Chatterjee, M. S. El Fallah, J. Ribas and S. K. Kar, *Polyhedron*, 2014, **68**, 212-221.
12. C.-B. Tian, Z.-H. Li, J.-D. Lin, S.-T. Wu, S.-W. Du and P. Lin, *Eur. J. Inorg. Chem.*, 2010, 427-437.
13. P. Bhunia, D. Banerjee, P. Datta, P. Raghavaiah, A. M. Z. Slawin, J. D. Woollins, J. Ribas and C. Sinha, *Eur. J. Inorg. Chem.*, 2010, 311-321.
14. S. Naiya, C. Biswas, M. G. B. Drew, C. J. Gomez-Gracia and A. Ghost, *Inorg. Chim. Acta*, 2011, **377**, 26-33.
15. M. Cheng, D. Lu, E.-Q. Gao and Q.-X. Jia, *Z. Anorg. Allg. Chem.*, 2015, **641**, 1258-1262.
16. (a) F. Liu, P. Li, W. Gao, X.-M. Zhang and J.-P. Liu, *Inorg. Chim. Acta*, 2016, **451**, 116-122; (b) M. Cheng, Y.-S. Ding, Z. Zhang and Q.-X. Jia, *Inorg. Chim. Acta*, 2016, **450**, 1-7.
17. C. Adhikary and S. Koner, *Coord. Chem. Rev.*, 2010, **254**, 2933-2958.
18. (a) T. K. Maji, P. S. Mukherjee, S. Koner, G. Mostafa, J.-P. Tuchagues, N. R. Chaudhuri, *Inorg. Chim. Acta*, 2001, **314**,111-116; (b) S. Mukherjee and P. S. Mukherjee, *Inorg. Chem.*, 2010, **49**, 10658-10667.

19. Z.-G. Gu, Y.-F. Xu, X.-J. Yin, X.-H. Zhou, J.-L. Zuo and X.-Z. You, *Dalton Trans.*, 2008, 5593-5602.
20. Y. S. You, J. H. Yoon, H. C. Kim and C. S. Hong, *Chem. Commun.*, 2005, 4116-4118.
21. M. S. A. Goher and F. A. Mautner, *J. Chem. Soc., Dalton Trans.*, 1999, 1535-1536.
22. K. C. Mondal and P. S. Mukherjee, *Inorg. Chem.*, 2008, **47**, 4215-4225.
23. S. Muhherjee and P. S. Mukherjee, *Dalton Trans.*, 2013, **42**, 4019-4030.
24. W.-B. Shi, A.-L. Cui and H.-Z. Kou, *Cryst. Growth Des.*, 2012, **12**, 3436-3443.
25. Z.-L. You, Q.-Z. Jiao, S.-Y. Niu, N.-Y. Chi, *Z. Anorg. Allg. Chem.*, 2006, **632**, 2481-2485.
26. N. Aiswarya, M. Sithambaresan, S. S. Sreejith, S. W. Ne and M. R. P. Kurup, *Inorg. Chim. Acta*, 2016, **443**, 251-266.
27. (a) A. Bhattacharyya and S. Chattopadhyay, *RSC Advances*, 2015, **5**, 18252-18257; (b) P. Charkraborty, I. Majumder, S. K. Chattopadhyay, E. Zangrando and D. Das *Inorg. Chim. Acta*, 2015, **436**, 139-145.
28. B.-D. Wu, Z,-N. Zhou, F.-G. Li, L. Yang, T.-L. Zhang and J.-G. Zhanga, *New J. Chem.*, 2013, **37**, 646-653.
29. (a) P. Bhowmik, A. Bhattacharyya, K. Hams, S. Sproules and S. Chattopadhyay, *Polyhedron*, 2015, **85**, 221-231; (b) S. Jana, B. K. Show, P. Bhowmik, K. Hams, M. G. B. Drew, S. Chattopadhyay and S. K. Saha, *Inorg. Chem.*, 2014, **53**, 8723-8734.
30. S. Muhherjee, Y. P. Patil and P. S. Mukherjee, *Dalton Trans.*, 2012, **41**, 54-64.
31. S. Naiya, C. Biswas, M. G. B. Drew, C. J. Gómez-García, J. M. Clemente-Juan and A. Ghosh, *Inorg. Chem.*, 2010, **49**, 6616-6627.
32. (a) S. Banerjee, C. Rizzoli and C. Adhikary, *Inorg. Chim. Acta*, 2013, **409**, 202-207; (b) R. Bera, C. Adhikary, S. Ianelli, S. Chudhuri and S. Koner, *Polyhedron*, 2010, **29**, 2166-2170.
33. C.-B. Tian, Z.-H. Li, J.-D. Lin, S.-T. Wu, S.-W. Du, P. Lin, *Eur. J. Inorg. Chem.*, 2010, 427-437.
34. (a) P. S. Mukherjee, T. K. Maji, A. Escuer, R. Vicente, J. Ribas, G. Rosair, F. A. Mautner and N. R. Chaudhuri, *Eur. J. Inorg. Chem.*, 2002, 943-949; (b) A. Esuer, M. Font-Bardia, E. Penalba, X. Solans and R. Vicente, *Inorg. Chim. Acta*, 2000, **298**, 195-201.
35. S. Sasmal, S. Sarkar, N. Aliaga-Alcalde and S. Mohanta, *Inorg. Chem.*, 2011, **50**, 5687-5695.
36. B. Kharediya and S. Sunkari, *Polyhedron*, 2013, **61**, 80-86.
37. Z. G. Gu, J.-J. Na; B.-X. Wang, H.-P. Xiao and Z. Li, *CrystEngComm*, 2011, **13**, 6415-6421.
38. A. Chakraborty, L. S. Rao, A. K. Manna, S. K. Pati, J. Ribas and T. K. Maji, *Dalton Trans.*, 2013, **42**, 10707-10717; (b) Y.-P. Diao, *Acta Crystallogr. Sect. E.: Struct. Rep. Online*, 2007, **63**, m1081.
39. (a) S. Sasmal, P. Chakraborty, S. Bhattacharya, N. Aliaga-Alcalde and S. Mohanta, *Polyhedron*, 2014, **73**, 67-71; (b) O. L. Casagrande Junior, S. I. Klein, A. E. Mauro and K. Tomita, *Transition Met. Chem.*, 1989, **14**, 45-47.
40. D. Ghoshal, T. M. Maji, E. Zangrando, T. Mallah, E. Riviere and N. R. Chaudhuri, *Inorg. Chim. Acta*, 2004, **357**, 1031-1038.
41. Y. Xie, Q. Liu, H. Jiang, C. Du, X. Xu, M. Yu and Y. Zhu, *New J. Chem.*, 2002, **26**, 176-179.
42. S. Mukhrejee, B. Gole, R. Chakrabarty and P. S. Mukherjee, *Inorg. Chem.*, 2009, **48**, 11325-11334.

43. A. Escuer, M. Font-Bardia, E. Penãlba, X. Solans and R. Vicente, *Polyhedron*, 1999, **18**, 211-215.
44. I. Bkouche-Waksman, S. Sikorav and O. Khan, *J. Crystallogr. Spectrosc. Res.*, 1983, **13**, 303-310.
45. P. Bkhowmik, S. Biswas, S. Chattopadhyay, C. Diaz, C. J. Gomez-Gracia and A. Ghosh, *Dalton Trans.*, 2014, **43**, 12414-12421.
46. (a) F. A. Mautner, C. Berger, R. C. Fischer and S. S. Massoud, *Inorg. Chim. Acta*, 2016, **439**, 69-76; (b) F. A. Mautner, M. Scherzer, C. Berger, R. C. Fischer and S. S. Massoud, *Inorg. Chim. Acta*, 2015, **425**, 46-51.
47. (a) M. Monfort, I. Resino, J. Ribas, X. Solans and M. Font-Bardia, *New J. Chem.*, 2001, **25**, 1577-1582; (b) M. Monfort, I. Resino, J. Ribas, X. Solans and H. Stoeckli-Evans, *Angew. Chem., Int. Ed.*, 2000, **39**, 191-193.
48. J. Boonmak, M. Nakano, N. Chaichit, C. Pakawatchai, Y. Youngme, *Inorg. Chem.*, 2011, **50**, 7324-7333.
49. (a) X.-T. Wang, X.-H. Wang, Z.-M. Wang and S. Gao, *Inorg. Chem.*, 2009, **48**, 1301-1308; (b) J.-P. Zhao, B.-W. Hu, E.C. Sanudo, Q. Yang, Y.-F. Zeng and X.-H. Bu, *Inorg. Chem.*, 2009, **48**, 2482-2489.
50. A. N. Georgopoulou, C. R. Raptopoulou, V. Psycharis, R. Ballesteros, B. Abarca and A. K. Boudlais, *Inorg. Chem.*, 2009, **48**, 3167-3176.
51. (a) J. Cano, F. A. Mautner, C. Berger, R. C. Fischer and R. Vicente, *Polyhedron*, 2013, **50**, 240-245; (b) F. A. Mautner, B. Sudy, A. Egger, E. M. Mautner, A. Escuer and R. Vicente, *Inorg. Chem. Commun.*, 2012, **21**, 4-7.
52. S. Youngme, T. Chotkhun, N. Chaichit, G. A. van Albada and J. Reedijk, *Inorg. Chem. Commun.*, 2007, **10**, 843-848.
53. W. J. Geary, *Coord. Chem. Rev.*, 1971, **7**, 81-122.
54. (a) B. J. Hathaway, in G. Wilkinson, R. D. Gillard and J. A. McCleverty (Eds), in *Comprehensive Coordination Chemistry*, vol. 5, Pergamon, Press, Oxford, England, 1987, pp. 533-593; (b) M. Duggan, N. Ray, B. Hathaway, G. Tomlinson, P. Brint an K. Pelin, *J. Chem. Soc., Dalton Trans.*, 1980, 1342-1348.
55. B. N. Figgis, M. A. Hitchman, *Ligand Field Theory and its Applications*, Wiley-VCH, New York, 2000.
56. A. W. Addison, T. N. Rao, J. Reedijk; J. V. Rijin and G. C. Verschoor, *J. Chem. Soc., Dalton Trans.*,1984, 1349-1356.
57. S. Triki, C. J. Gómez-García, E. Ruiz and J. Sala-Pala, *Inorg. Chem.*, 2005, 44, 5501-5508.
58. L.-L. Ni, Z.-L. You, L. C. Wang and K. Li, *Transition. Met. Chem.*, 2010, **35**, 13-17.
59. A. Ray, S. Banerjee, R. J. Butcher, C. Desplanches and S. Mitra, *Polyhedron*, 2008, **27**, 2409-2415.
60. M. S. Ray, A. Ghosh, R. Bhattacharya, G. Mukhopadhyay, M. G. B. Drew and J. Ribas, *Dalton Trans.*, 2004, 252-259.
61. N. F. Chilton, R. P. Anderson, L. D. Turner, A. Soncini and K. S. Murray, *J. Comput. Chem.*, 2013, **34**, 1164-1175.
62. Y. Agnus, R. Louis, J.-P. Gisselbrecht, R. Weiss, *J. Am. Chem. Soc.*, 1984, **106**, 93-102.
63. P. Chauduri, K. Oder, K. Wieghardt, B. Nuber, J. Weiss, *Inorg. Chem.*, 1986, **25**, 2818-2824.
64. E. Ruiz, J. Cano, S. Alvarez and P. Alemany, *J. Am. Chem. Soc.*, 1998, **120**, 11122-11129.

65. R. M. Martin, *Electronic Structure, Basic Theory and Practical Methods*, Cambridge University Press, Cambridge, 2004.
66. J. M. Soler, E. Artacho, J. D. Gale, A. Garcia, J. Junquera, P. Ordejon and D. Sanchez-Portal, *J. Phys-Cond. Matter*, 2002, **14**, 2745-2779.
67. D. Sánchez-Portal, P. Ordejón and E. Canadell, in *Principles and Applications of Density Functional Theory in Inorganic Chemistry II*, Springer Berlin Heidelberg, Berlin, Heidelberg, 2004, pp. 103-170.
68. J. P. Perdew, K. Burke and M. Ernzerhof, *Phys. Rev. Lett.*, 1996, **77**, 3865-3868.
69. A. I. Liechtenstein, V. I. Anisimov and J. Zaanen, *Physical Review B*, 1995, **52**, R5467-R5470.
70. E. Ruiz, *Exchange Coupling in Di- and Polynuclear Systems* in *Comprehensive Inorganic Chemistry II (Second Edition)*, Ed. J. R. Poeppelmeier, Elsevier, Amsterdam, 2013, pp. 501-549.
71. N. Trouiller and J. L. Martins, *Phys. Rev. B*, 1991, **43**, 1993-2996.
72. L. Kleinman and D. M. Bylander, *Phys. Rev. Lett.*, 1982, **48**, 1425-1428.
73. E. Ruiz, A. Rodríguez-Fortea, J. Tercero, T. Cauchy and C. Massobrio, *J. Chem. Phys.*, 2005, **123**, 074102.
74. E. Ruiz, M. Llunell and P. Alemany, *J. Sol. State Chem.*, 2003, **176**, 400-411.
75. A. Escuer and G. Aromí, *Eur. J. Inorg. Chem.*, 2006, 4721-4736.
76. (a) Bruker (2005) SAINT v. 7.23; Bruker (2006) APEX 2, v. 2.0-2; Bruker AXS Inc. Madison, Wisconsin, USA; (b) G. M. Sheldrick (2001), SADABS v. 2. University of Goettingen, Germany.
77. (a) G. M. Sheldrick, *Acta Crystallogr.*, 2008, **A64**, 112-122; (b) G. M. Sheldrick, *Acta Crystallogr.*, 2015, **C71**, 3-8.
78. C. F. Macrae, P. R. Edington, P. McCabe, E. Pidcock, G. P. Shields, R. Taylor, T. Towler, and J. van de Streek, *J. Appl. Crystallogr.*, 2006, **39**, 453-547.
79. A. W. Sandvik, *Phys. Rev. B*, 1999, **59**, R14157-R14160.
80. A. F. Albuquerque, F. Alet, P. Corboz, P. Dayal, A. Feiguin, S. Fuchs, L. Gamper, E. Gull, S. Gürtler, A. Honecker, R. Igarashi, M. Körner, A. Kozhevnikov, A. Läuchli, S. R. Manmana, M. Matsumoto, I. P. McCulloch, F. Michel, R. M. Noack, G. Pawlowski, L. Pollet, T. Pruschke, U. Schollwöck, S. Todo, S. Trebst, M. Troyer, P. Werner and S. Wessel, *J. Magn. Mat.*, 2007, **310**, 1187-1193.
81. B. Bauer, L. D. Carr, H. G. Evertz, A. Feiguin, J. Freire, S. Fuchs, L. Gamper, J. Gukelberger, E. Gull, S. Guertler, A. Hehn, R. Igarashi, S. V. Isakov, D. Koop, P. N. Ma, P. Mates, H. Matsuo, O. Parcollet, G. Pawłowski, J. D. Picon, L. Pollet, E. Santos, V. W. Scarola, U. Schollwöck, C. Silva, B. Surer, S. Todo, S. Trebst, M. Troyer, M. L. Wall, P. Werner, S. Wessel, *J. Stat. Mech. Theor. Exp.*, 2011, P05001.PLEASE CHECK!